

Oxygen isotope zoning in garnets from Franciscan eclogite blocks: evidence for rock–buffered fluid interaction in the mantle wedge

Jessica C. Errico · Jaime D. Barnes ·
Ariel Strickland · John W. Valley

Received: 1 February 2013 / Accepted: 19 June 2013 / Published online: 6 July 2013
© Springer-Verlag Berlin Heidelberg 2013

Abstract The oxygen isotope compositions of eclogite and amphibolite garnets from Franciscan Complex high-grade blocks and actinolite rinds encasing the blocks were determined to place constraints on their fluid histories. SIMS oxygen isotope analysis of single garnets from five eclogite blocks from three localities (Ring Mountain, Mount Hamilton, and Jenner Beach) shows an abrupt decrease in the $\delta^{18}\text{O}$ value by $\sim 1\text{--}3\text{‰}$ from core to rim at a distance of $\sim 120 \pm 50\ \mu\text{m}$ from the rim in nine out of the 12 garnets analyzed. In contrast, amphibolite garnets from one block (Ring Mountain) analyzed show a gradual increase in $\delta^{18}\text{O}$ value from core to rim, implying a different history from that of the eclogite blocks. Values of $\delta^{18}\text{O}$ in eclogite garnet cores range from 5.7 to 11.6 ‰, preserving the composition of the eclogite protolith. The abrupt decrease in the $\delta^{18}\text{O}$ values of the garnet rims to values ranging from 3.2 to 11.2 ‰ suggests interaction with a lower $\delta^{18}\text{O}$ fluid during the final stages of growth during eclogite facies metamorphism (450–600 °C). We hypothesize that this fluid is sourced from the serpentinized mantle wedge. High Mg, Ni, and Cr contents of actinolite rinds encasing the blocks also support interaction with ultramafic

rock. Oxygen isotope thermometry using chlorite and phengite versus actinolite of rinds suggests temperatures of 185–240 °C at Ring Mountain and Mount Hamilton. Rind formation temperatures together with the lower $\delta^{18}\text{O}$ garnet rims suggest that the blocks were in contact with ultramafic rock from the end of garnet growth through low-temperature retrogression. We suggest a tectonic model in which oceanic crust is subducted at the initiation of subduction and becomes embedded in the overlying mantle wedge. As subduction continues, metasomatic exchange between high-grade blocks and surrounding ultramafic rock is recorded in low $\delta^{18}\text{O}$ garnet rims, and later as temperatures decrease, with rind formation.

Keywords Franciscan Complex · Eclogite · Garnet · Oxygen isotopes · SIMS

Introduction

Fluids are a primary means of mass transport in subduction zones with major consequences of arc magmatism, seismicity, and the chemical evolution of the crust and mantle. Tracing fluid pathways, sources, and compositional evolution during subduction is critical to understanding this transport process. Globally, many subduction zones preserve obducted metamorphic complexes containing high-grade blocks of varying P–T conditions (e.g., eclogites, blueschists, amphibolites) in a subduction-related mélange matrix ranging from pelitic to ultramafic in composition (e.g., Franciscan Complex, CA; Catalina Schist, CA; Syros, Greece; Samana Metamorphic Complex, Dominican Republic; New Caledonia) (e.g., Cloos 1986; Sorensen et al. 1997; Breeding et al. 2004; Bebout and Barton 1989, 1993, 2002; Spandler et al. 2004). These exposed

Communicated by T. L. Grove.

Electronic supplementary material The online version of this article (doi:10.1007/s00410-013-0915-0) contains supplementary material, which is available to authorized users.

J. C. Errico (✉) · J. D. Barnes
Jackson School of Geosciences, University of Texas,
Austin, TX 78712, USA
e-mail: jessica.errico@gmail.com

A. Strickland · J. W. Valley
Department of Geoscience, WiscSIMS, University of Wisconsin,
Madison, WI 53706, USA

complexes are ideal natural laboratories for studying fluid processes in subduction zones.

In this study we focus on the Franciscan Complex of California, where extensive previous geochemical work on high-grade blocks has demonstrated significant involvement of fluids at depth within the subduction zone (Nelson 1991, 1995; Giaramita and Sorensen 1994; Sorensen et al. 1997; Catlos and Sorensen 2003; Horodyskyj et al. 2009; Penniston-Dorland et al. 2010; Simons et al. 2010). The Franciscan Complex is an accretionary prism, formed during the subduction of the Pacific plate beneath the North American plate from the late Jurassic through the Oligocene. The classic Franciscan “mélange” typically refers to the Central Belt, a highly deformed and sheared shale matrix mélange containing rare, but well-studied high-grade blocks of blueschist, eclogite, and amphibolite (Bailey et al. 1964; Cloos 1986; Blake et al. 1988; Krogh Ravn and Terry 2004; Tsujimori et al. 2006; Page et al. 2007). These high-grade blocks are also of interest because they show evidence for a complex history from igneous crystallization and peak eclogite metamorphism through multiple overprinting events (e.g., blueschist retrogression, actinolite rind) while partially preserving their peak metamorphic assemblage (Cloos 1986; Moore 1984; Krogh et al. 1994). Much research has focused on determining the mechanism(s) responsible for exhuming these high-grade blocks while avoiding complete retrogression (e.g., Platt 1986; Cloos 1982, 1985; Moore 1984; Horodyskyj et al. 2009).

Metasomatic rinds are a common feature of Franciscan high-grade blocks, as well as blocks from other mélange units (e.g., Catalina Schist; Syros; Dominican Republic) (e.g., Moore 1984; Cloos 1986; Sorensen et al. 1997; Breeding et al. 2004; Bebout and Barton 1993, 2002). In the Franciscan, the rind is characterized by the presence of actinolite and chlorite on the block edges and along some fractures. It is commonly believed that the rind formed from interaction between the blocks and surrounding ultramafic rock because of the high Mg, Ni, and Cr concentrations in the rind; however, the timing and temperature of rind formation are not well constrained (Moore 1984; Cloos 1986; Coleman and Lanphere 1971; Giaramita and Sorensen 1994; Horodyskyj et al. 2009).

The prograde and retrograde minerals preserved in these high-grade blocks, as well as the hydrous minerals in the actinolite rind, have the potential to record an evolving fluid history in a subduction zone from initiation through maturity that can be deciphered using stable isotopes. Here, we use laser fluorination (bulk samples) and in situ secondary ion mass spectrometry (SIMS) measurements of oxygen isotope ratios of minerals from six (five eclogites and one amphibolite) high-grade Franciscan blocks (Ring Mountain, Jenner Beach, and Mount Hamilton) to constrain the nature of the fluids and the temperature of retrogression

of the blocks. Surprisingly, despite extensive geochemical studies of Franciscan high-grade blocks (Nelson 1991, 1995; Giaramita and Sorensen 1994; Sorensen et al. 1997; Catlos and Sorensen 2003; Horodyskyj et al. 2009; Penniston-Dorland et al. 2010; Simons et al. 2010) and the use of oxygen isotopes to successfully decipher fluid histories and mobility in other exhumed subducted metamorphic complexes (e.g., Halama et al. 2011; Putlitz et al. 2000; Bebout and Barton 1989), only a handful of studies (Taylor and Coleman 1968; Page et al. 2010b; Pincus et al. 2010) utilize oxygen isotopes to interpret the fluid histories of Franciscan high-grade blocks. New oxygen isotope data presented here will be used to determine the metasomatic history of Franciscan blocks and the timing of actinolite rind formation, ultimately allowing for an improved understanding of the tectonic evolution of the subduction zone.

Geologic background

The Franciscan Complex (Fig. 1) formed during the eastward dipping subduction of the Pacific plate beneath the North American plate from the late Jurassic through the Oligocene (Hamilton 1969; Blake et al. 1988). It is subdivided into three NNW trending belts (Eastern Belt, Central Belt, Coastal Belt) decreasing in age and metamorphic grade from east to west (Bailey and Irwin 1959; Bailey et al. 1964). The Central Belt mélange is a host to numerous exotic blocks of low-grade graywacke, greenstones, chert, rare limestone, variably serpentized ultramafic rocks, and high-grade blocks (eclogite, blueschist, and amphibolite), the focus of this study (Bailey et al. 1964; Cloos 1986; Blake et al. 1988).

Franciscan high-grade blocks are locally exposed in sea cliffs or protruding out of the grassy hill slopes. Block–matrix contacts are rarely observed, but where seen, the matrix is shale (Bailey et al. 1964; Cloos 1986; Moore and Blake 1989). Major and trace element trends and Sr and Nd isotope data suggest a mid-ocean ridge basalt (MORB) or enriched MORB protolith (e.g., Moore and Blake 1989; Nelson 1991, 1995; Krogh et al. 1994; Sorensen et al. 1997; Horodyskyj et al. 2009). Eclogites are suggested to have followed a counterclockwise P–T path (Fig. 2) attributed to a decreasing geothermal gradient caused by the continued subduction of cold oceanic lithosphere (Cloos 1982, 1985; Krogh et al. 1994; Ukar 2012). The blocks are estimated to have reached peak amphibolite (500–650 °C) to eclogite (450–600 °C) facies conditions between ~159 and 140 Ma (Coleman and Lanphere 1971; Cloos 1985; Anczkiewicz et al. 2004; Page et al. 2007), shortly after the initiation of subduction. Pressure estimates vary between 8 and 25 kbar corresponding to depths

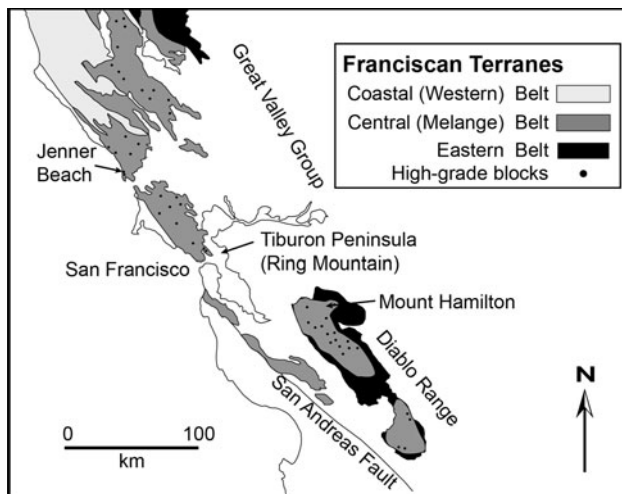


Fig. 1 Generalized geologic map of central California showing the Coastal, Central, and Eastern belts of the Franciscan Complex and the three sample locations from this study (Ring Mountain, Jenner Beach, and Mount Hamilton). High-grade blocks are not to scale, and locations are generalized. Modified from Coleman and Lanphere (1971) and Cloos (1986)

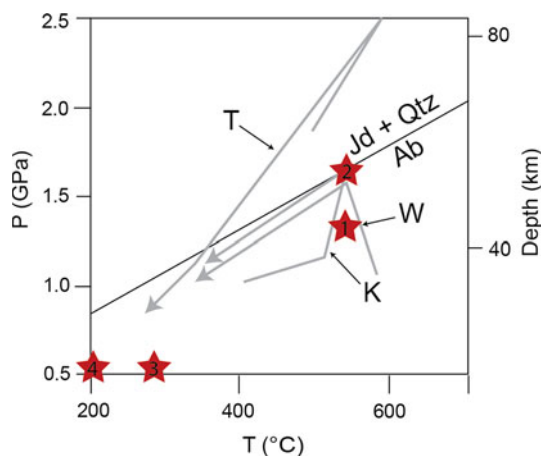


Fig. 2 Gray arrows indicate P–T paths of Franciscan eclogites defined by T = Tsujimori et al. (2006), W = Wakabayashi (1990), and K = Krogh et al. (1994). Eclogite blocks from Ring Mountain were used in the Tsujimori et al. (2006) and the Wakabayashi's (1990) studies. Jenner Beach eclogites were used in the Krogh et al. study. The red numbered stars coordinate with the model stages b–e in Fig. 7

between 25 and 80 km (e.g., Moore 1984; Moore and Blake 1989; Wakabayashi 1990; Krogh et al. 1994; Tsujimori et al. 2006; Page et al. 2007). It is suggested that the high-grade blocks were underplated in the mantle wedge (Cloos 1982; Ukar 2012) and due to “refrigeration” of the hanging wall experienced a retrograde blueschist overprint between 300 and 350 °C (Tsuji-mori et al. 2006; Wakabayashi 1990). Assent rates between 2 and 5 km/Ma have been suggested corresponding to ~20 Ma between peak metamorphism and exhumation, potentially explaining the

partial preservation of the peak amphibolite/eclogite assemblage (Cloos 1985; Anczkiewicz et al. 2004; Horodyskyj et al. 2009).

Three main mechanisms have been proposed to explain the movement of Franciscan high-grade blocks from depth to their current position in the mélangé. Geochemical evidence of interaction with serpentinites and proximity between the high-grade blocks and serpentinites in the field has led to the first model: High-grade blocks are carried to the surface in a buoyant serpentinite diapir/channel (e.g., Ernst 1970; Moore 1984; Horodyskyj et al. 2009). The second model describes flow dynamics within an accretionary prism to explain the chaotic occurrence pattern of the high-grade blocks. This model, known as return or corner flow, proposes that convective motion driven by the subducting plate carries blocks from depth back to shallow levels within the prism (Cloos 1982). The third model is rooted in the structural evolution of the accretionary prism: High P/T blocks are brought to the upper levels of the accretionary prism along extension-induced listric normal faults caused by the underplating of materials at the base of the wedge (e.g., Platt 1986; Jayko et al. 1987; Harms et al. 1992; Ring and Brandon 1994; Schemmann et al. 2008). A consensus regarding these models has not been reached.

Eclogite, blueschist, and amphibolite blocks of the Franciscan record evidence of fluid–rock interaction at depths within the subduction zone. Despite the ambiguity of the high-grade block–matrix relationship, many authors suggest that the blocks interacted with serpentinite or serpentinite-derived fluid based on their preserved Mg-, Cr-, and Ni-rich actinolite rinds (Moore 1984; Cloos 1986; Coleman and Lanphere 1971; Giaramita and Sorensen 1994; Horodyskyj et al. 2009). In addition to major and trace element geochemical evidence for interaction with serpentinite, Franciscan blocks show significant major and trace element geochemical evidence for interaction with sediments or sediment-derived fluids (Sorensen et al. 1997; Nelson 1991, 1995; Horodyskyj et al. 2009; Penniston-Dorland et al. 2010; Simons et al. 2010). Low ϵNd values of vein and rind material relative to block cores of Franciscan blueschist and eclogite blocks suggest that sediment-derived fluids were involved in rind formation and as through-going fluids (Nelson 1991, 1995). Enrichments in large-ion lithophile elements (LILE), such as Cs, Rb, Ba, K, and Tl, in blocks and rinds from several Franciscan localities including Ring Mountain suggest interaction with sediment-derived fluids (Sorensen et al. 1997; Catlos and Sorensen 2003; Horodyskyj et al. 2009). High whole-rock Li concentrations and low $\delta^7\text{Li}$ values of Franciscan eclogites relative to MORB, the presumed protolith, also suggest rehydration of the blocks with a fluid containing a sediment-derived component during retrogression (Penniston-Dorland et al. 2010; Simons et al. 2010).

Sample descriptions

Samples from three well-known Franciscan high-grade block localities were analyzed in this study, Ring Mountain, Jenner Beach, and Mount Hamilton. All samples show evidence of minor to moderate lower-temperature retrogression through the replacement of the peak assemblage minerals (e.g., garnet, hornblende, Na-rich pyroxene) by Na-rich amphibole and chlorite and, on some blocks, the development of an actinolite rind. A summary of all samples, their location, modal mineralogy, and the types of stable isotope analyses made is provided in Table 1.

Ring Mountain

Ring Mountain is located on Tiburon Peninsula near its northern junction with the mainland (Fig. 1). The Franciscan rocks exposed on Tiburon Peninsula include graywacke, shale, conglomerate, chert, serpentinite, metabasalt, and isolated high-grade blocks of eclogite, blueschist, and amphibolite (Page 1968). The high-grade blocks are isolated, jut out of grassy hill slopes, and lack evidence of their original matrix association. They range in size from 1 to 2 m in height and 2 to 3 m in width. Eclogite and actinolite rind samples from one block and amphibolite samples from a second block were provided by C.-T. Lee. These are the same samples and sample names used by Horodyskyj et al. (2009). Two additional actinolite rind samples not used in the Horodyskyj et al.'s (2009) study (RM-11-5A and UH4) from the eclogite block have been used in this study.

Jenner beach

Jenner beach is located directly north of the mouth of the Russian River, approximately 55 miles north of San Francisco (Fig. 1). Eclogite, blueschist, and greenstone blocks are exposed on the beach and in the sea cliffs. The blocks range in size from small boulders (0.5 m in diameter) up to several meters in diameter. The high-grade blocks are interlayered eclogite/blueschist with preserved actinolite rinds. Three high-grade blocks and actinolite rind on an eclogite layer were sampled along the beach as a part of this study.

Mount Hamilton

The Mount Hamilton eclogite block has been destroyed by roadwork. Samples for this study have been provided by Mark Cloos and were previously studied in the thesis of Herrington (1985); sample names have not been changed. Sample MH-9 is eclogite from the core of the block consisting of garnet and omphacite with minor amounts of

white mica and rutile. Samples MH-8 and MH-10 are characterized by partial replacement of omphacite by Na-amphibole and were collected closer to the edges of the block. Sample MH-6 is actinolite rind collected from the surface of the block.

Analytical procedures

Sample preparation

Garnet mineral separates were prepared for bulk oxygen isotope analysis (laser fluorination) by hand crushing and sieving (Standard US Sieve Size 60, 250 μm) and washing approximately 10 g of sample. Individual mineral grains were then handpicked using a binocular microscope with an estimated visual clarity of 90 %.

Garnets analyzed using the ion microprobe were extracted as intact euhedral garnets from hand-crushed rock sample. They were then grouped by size (~ 1 mm in diameter and ~ 0.5 mm in diameter) and cast in two 25-mm epoxy disks according to size. They were hand polished to achieve as close to central sections as possible. Both mounts include multiple grains of the UWG-2 garnet standard (Valley et al. 1995) in the center of the mount. All garnet standards and samples were mounted within 5 mm of the center of the epoxy disk.

Laser fluorination

Oxygen was extracted from ~ 2 mg of the hand-separated mineral grains by the laser fluorination technique of Sharp (1990). Samples were individually heated by a CO_2 laser in the presence of BrF_5 and then cryogenically purified using the silicate extraction line at the University of Texas at Austin. Once the oxygen was purified, the $\delta^{18}\text{O}$ values were determined using a ThermoElectron MAT 253 mass spectrometer. The following standards were used to ensure precision and accuracy: garnet standard UWG-2 ($\delta^{18}\text{O} = +5.8$ ‰) (Valley et al. 1995) and in-house quartz standards Gee Whiz ($\delta^{18}\text{O} = +12.6$ ‰) and Lausanne-1 ($\delta^{18}\text{O} = +18.1$ ‰). $\delta^{18}\text{O}$ values are reported relative to SMOW, where the $\delta^{18}\text{O}$ value of NBS-28 is $+9.65$ ‰. Error is ± 0.1 ‰. Results are presented in Table 2.

Ion microprobe

Oxygen isotope analysis was performed at the University of Wisconsin WiscSIMS laboratory using a CAMECA IMS-1280 ion microprobe following the procedures outlined in Page et al. (2010a), Kita et al. (2009), and Valley and Kita (2009). A focused $^{133}\text{Cs}^+$ primary beam was used for analysis at 1.6–2.2 nA and a corresponding spot size of

Table 1 Sample description and summary

Sample name	Sample location	Rock type	Mineralogy (modal %) ^a	Bulk ^b	SIMS ^b
Ring Mountain					
UH-1	N37°54.731' W122°29.118'	Eclogite	gar (35 %) + Na-pyx (55 %) + Na-amph (5 %) ± ep ± tit ± chl ± rut ± Fe-ox	2	2
UH-8	N37°54.731' W122°29.118'	Eclogite	gar (35 %) + Na-pyx (55 %) + Na-amph (5 %) ± ep ± tit ± chl ± rut ± Fe-ox	2	
UH-3	N37°54.731' W122°29.118'	Amphibolite	gar (20 %) + amph (45 %) + ep (20 %) + chl (10 %) + white mica (4 %) ± rut ± Fe-ox	1	2
UH-6	N37°54.731' W122°29.118'	Amphibolite	gar (20 %) + amph (47 %) + ep (20 %) + chl (10 %) + white mica (2 %) ± rut ± Fe-ox	3	1
UH-10	N37°54.731' W122°29.118'	Amphibolite	gar (20 %) + amph (45 %) + ep (20 %) + chl (10 %) + white mica (4 %) ± rut ± Fe-ox	2	
UH-11	N37°54.731' W122°29.118'	Amphibolite	gar (20 %) + amph (45 %) + ep (20 %) + chl (10 %) + white mica (4 %) ± rut ± Fe-ox	1	
UH-12	N37°54.731' W122°29.118'	Amphibolite	gar (20 %) + amph (45 %) + ep (20 %) + chl (10 %) + white mica (4 %) ± rut ± Fe-ox	1	1
UH-4	N37°54.731' W122°29.118'	Actinolite rind	act (95 %) + chl (5 %)	1	
RM11-5A	N37°54.730' W122°29.117'	Actinolite rind	act (93 %) + wm (5 %) + chl (2 %)	5	
Jenner beach					
JEN11-1C	N38°27.207' W123°07.977'	Eclogite	gar (25 %) + Na-pyx (45 %) + Na-amph (5 %) + ep (5 %) + tit (5 %) + chl (5 %) ± rut ± Fe-ox	3	1
JEN11-1D	N38°27.207' W123°07.977'	Eclogite	gar (25 %) + Na-pyx (45 %) + Na-amph (5 %) + ep (5 %) + tit (5 %) + chl (5 %) ± rut ± Fe-ox	2	1
JEN11-2B	N38°27.180' W123°07.920'	Eclogite	gar (25 %) + Na-pyx (45 %) + Na-amph (5 %) + ep (5 %) + tit (5 %) + chl (5 %) ± rut ± Fe-ox	2	
JEN11-2D	N38°27.180' W123°07.920'	Eclogite	gar (25 %) + Na-pyx (45 %) + Na-amph (5 %) + ep (5 %) + tit (5 %) + chl (5 %) ± rut ± Fe-ox	2	
JEN11-3C	N38°27.153' W123°07.826'	Eclogite	gar (25 %) + Na-pyx (45 %) + Na-amph (5 %) + ep (5 %) + tit (5 %) + chl (5 %) ± rut ± Fe-ox	2	2
JEN11-2D	N38°27.180' W123°07.920'	Actinolite rind	act (95 %) + chl (5 %)	3	
Mount Hamilton					
MH-8		Eclogite	gar (13 %) + Na-pyx (8 %) + amph (75 %) + white mica (3 %) ± tit ± chl ± rut		2
MH-9		Eclogite	gar (23 %) + Na-pyx (73 %) + white mica (3 %) + rut (1 %)		2
MH-10		Eclogite	gar (13 %) + Na-pyx (8 %) + amph (75 %) + white mica (3 %) ± tit ± chl ± rut		2
MH-6		Actinolite rind	act (97 %) + white mica (3 %) ± rut	3	

Data given in Table 2

^a gar = garnet; Na-pyx = Na-rich pyroxene; Na-amph = Na-rich amphibole; ep = epidote; tit = titanite; rut = rutile; Fe-ox = Fe-oxide. Data from this study, Horodyskyj et al. (2009) and Herrington (1985). Modal % is a visual estimation based on the method of Compton (1962)

^b Summary of the type of stable isotope analysis made. Bulk = number of individual analyses performed on mineral separates from each sample by laser fluorination. SIMS = number of individual garnets analyzed using the ion microprobe per sample

~12 μm. A normal-incidence electron gun was used for charge compensation of gold-coated samples. The secondary-ion accelerating voltage was set at 10 kV, and the oxygen ions were collected in two Faraday cups simultaneously. Prior to analysis, a set of eight garnet standards were analyzed, and their grossular content was used to

generate a compositional correction after Page et al. (2010a; see Appendix A on supplementary material). Four consecutive measurements of garnet standard UWG-2 ($\delta^{18}\text{O} = 5.8 \text{ ‰}$, Valley et al. 1995) were analyzed at the beginning and end of each session, and every 10–20 unknowns throughout each session. The average values of

Table 2 Oxygen isotope data for mineral separates from eclogite, amphibolite, and rind samples determined by laser fluorination

	Ring Mountain $\delta^{18}\text{O}$ values (‰ vs. SMOW)									
	Eclogite		Actinolite rind		Amphibolite					
	UH1	UH8	UH4	RM11-5A	UH3	UH6	UH10	UH11	UH12	
Garnet	6.9	7.2			8.3	8.3	8.0	8.1	8.5	
	6.7	7.0				8.4	7.9			
						8.2				
Actinolite			8.1	8.1						
				7.0						
				7.8						
Chlorite				7.7	7.9	8.1	7.8	8.0	7.8	
				7.4						
Phengite										
	Jenner beach $\delta^{18}\text{O}$ values (‰ vs. SMOW)					Mount Hamilton $\delta^{18}\text{O}$ values (‰ vs. SMOW)				
	Eclogite					Actinolite rind	Actinolite rind			
	JEN11-1C	JEN11-1D	JEN11-2B	JEN11-2D	JEN11-3C	JEN11-2D	MH6			
Garnet	10.0	9.8	10.1	10.8	10.7					
	10.2	10.5	10.0	8.6	11.3					
	8.8									
Actinolite						8.5	6.9			
						8.2	6.7			
							7.1			
Chlorite						9.6				
Phengite							9.2			

the standard analyses that bracket each set of unknowns were used in addition to the working curve for all eight garnet standards to correct for instrumental bias. The average precision (reproducibility) of the bracketing standards for this study ranged from ± 0.18 to ± 0.36 ‰ and averaged ± 0.3 ‰ (2SD). After oxygen isotope analysis, the ion microprobe pits were imaged using the scanning electron microscope and pits located on cracks or inclusions were excluded from the data set. Table 3 contains a summary of SIMS analyses, and Appendix A on supplementary material contains all raw and corrected SIMS data.

Electron microprobe

The cation geochemistry of garnets was determined using the JEOL JXA-8200 electron microprobe at the University of Texas at Austin. Garnets were analyzed in point-beam mode with an accelerating potential of 15 kV and 20 nA beam current. The count time was 15 s on peak for Mg, Mn, Fe, Al, and Si, 40 s on peak for Ca and Cr, and 8 s off peak for all elements. Three individual EMP points were analyzed per SIMS spot location. Natural and synthetic

silicate and oxide standards were used. Data were reduced using the Probe for Windows software (Donovan et al. 2007). Results are presented in Appendix B on supplementary material.

Results

Eclogite

Oxygen isotopes by laser fluorination

Bulk $\delta^{18}\text{O}$ values were obtained for two Ring Mountain garnets from one block (UH1 and UH8) and five Jenner Beach garnets from three blocks (JEN11-1C, JEN11-1D, JEN11-2B, JEN11-2D, and JEN11-3C). Garnets from Ring Mountain have similar $\delta^{18}\text{O}$ values of 6.8 ± 0.1 ‰ ($n = 2$) and 7.1 ± 0.1 ‰ ($n = 2$), respectively, whereas garnets from Jenner Beach have consistently higher $\delta^{18}\text{O}$ values of 9.5 ± 0.7 ‰ ($n = 3$), 10.2 ± 0.3 ‰ ($n = 2$), 10.1 ± 0.1 ‰ ($n = 2$), 9.7 ± 1.6 ‰ ($n = 2$), and 11.0 ± 0.3 ‰ ($n = 2$), respectively (Table 2; Fig. 3). A

Table 3 SIMS $\delta^{18}\text{O}$ values of core to rim transects of Franciscan garnets

Mount Hamilton eclogite					Mount Hamilton eclogite				
SIMS analysis no.	Distance from rim (μm) ^a	Sample name ^b	$\delta^{18}\text{O}$ ‰ VSMOW	2SD	SIMS analysis no.	Distance from rim (μm) ^a	Sample name ^b	$\delta^{18}\text{O}$ ‰ VSMOW	2SD
MH8-1 transect length: 316 μm					MH10-1 transect length: 461 μm				
248	316	MH8-1	8.5	0.3	255	461	MH10-1	8.2	0.3
252	253	MH8-1	8.5	0.3	257	389	MH10-1	8.2	0.3
254	211	MH8-1	8.6	0.3	261	356	MH10-1	8.1	0.3
251	147	MH8-1	9.1	0.3	262	333	MH10-1	8.5	0.3
253	95	MH8-1	6.5	0.3	256	311	MH10-1	6.4	0.3
250	53	MH8-1	5.8	0.3	260	233	MH10-1	5.4	0.3
249	16	MH8-1	5.3	0.3	259	144	MH10-1	5.3	0.3
MH8-5 transect length: 389 μm					258	22	MH10-1	5.3	0.3
157	389	MH8-5	8.4	0.2	MH10-7 transect length: 260 μm				
158	263	MH8-5	8.2	0.2	201	188	MH10-7	8.9	0.3
170	222	MH8-5	8.5	0.3	171	260	MH10-7	8.7	0.3
159	185	MH8-5	8.7	0.2	174	217	MH10-7	9.0	0.3
167	141	MH8-5	5.9	0.3	175	150	MH10-7	9.0	0.3
162	89	MH8-5	5.6	0.2	176	83	MH10-7	8.3	0.3
160	56	MH8-5	5.4	0.2	177	50	MH10-7	5.5	0.3
161	22	MH8-5	5.9	0.2	172	10	MH10-7	5.7	0.3
168	31	MH8-5	5.6	0.3	173	23	MH10-7	5.9	0.3
169	59	MH8-5	5.4	0.3	<i>Ring Mountain eclogites</i>				
MH9-1 transect length: 385 μm					UH1-7 transect length: 292 μm				
235	385	MH9-1	7.0	0.3	151	292	UH1-7	6.2	0.2
236	315	MH9-1	6.9	0.3	153	223	UH1-7	5.7	0.2
238	238	MH9-1	6.9	0.3	153	142	UH1-7	6.0	0.2
237	173	MH9-1	7.3	0.3	155	78	UH1-7	6.3	0.2
239	112	MH9-1	5.3	0.3	188	55	UH1-7	6.1	0.2
241	58	MH9-1	5.5	0.3	187	38	UH1-7	4.2	0.2
240	23	MH9-1	6.2	0.3	152	22	UH1-7	4.2	0.2
242	15	MH9-1	5.7	0.3	156	19	UH1-7	4.4	0.2
MH9-4 transect length: 307 μm					UH1-8 transect length: 363 μm				
192	307	MH9-4	7.2	0.2	189	363	UH1-8	5.7	0.2
196	200	MH9-4	7.1	0.2	204	126	UH1-8	5.9	0.3
195	150	MH9-4	7.3	0.2	202	74	UH1-8	4.4	0.3
194	107	MH9-4	6.2	0.2	203	37	UH1-8	4.1	0.3
193	21	MH9-4	6.6	0.2	190	70	UH1-8	5.7	0.2
					191	24	UH1-8	3.2	0.2
<i>Jenner Beach eclogite</i>					<i>Ring Mountain amphibolite</i>				
SIMS analysis no.	Distance from rim (μm) ^a	Sample name ^b	$\delta^{18}\text{O}$ ‰ VSMOW	2SD	SIMS analysis no.	Distance from rim (μm) ^a	Sample name ^b	$\delta^{18}\text{O}$ ‰ VSMOW	2SD
JEN11-3C-3 transect length: 542 μm					UH3-1 transect length: 900 μm				
129	542	JEN11-3C-3	11.4	0.4	270	900	UH3-1	5.7	0.3
135	396	JEN11-3C-3	11.3	0.3	269	750	UH3-1	6.2	0.3
136	269	JEN11-3C-3	11.1	0.3	267	442	UH3-1	7.2	0.3
137	138	JEN11-3C-3	10.6	0.3	272	258	UH3-1	8.0	0.3
130	27	JEN11-3C-3	9.7	0.4	271	150	UH3-1	8.2	0.3
139	5	JEN11-3C-3	10.0	0.3	268	33	UH3-1	8.5	0.3
138	31	JEN11-3C-3	11.0	0.3	UH3-3 transect length: 336 μm				

Table 3 continued

Jenner Beach eclogite					Ring Mountain amphibolite				
SIMS analysis no.	Distance from rim (μm) ^a	Sample name ^b	$\delta^{18}\text{O}$ ‰ VSMOW	2SD	SIMS analysis no.	Distance from rim (μm) ^a	Sample name ^b	$\delta^{18}\text{O}$ ‰ VSMOW	2SD
JEN11-1D-4 transect length: 206 μm					218	336	UH3-3	8.4	0.4
182	206	JEN11-1D-4	11.3	0.2	222	280	UH3-3	7.8	0.4
183	133	JEN11-1D-4	9.9	0.2	221	216	UH3-3	7.4	0.4
184	92	JEN11-1D-4	10.0	0.2	220	136	UH3-3	7.9	0.4
185	47	JEN11-1D-4	10.2	0.2	219	28	UH3-3	8.8	0.4
186	17	JEN11-1D-4	10.5	0.2	225	178	UH3-3	8.0	0.4
JEN11-1C-3 transect length: 305 μm					224	95	UH3-3	8.4	0.4
141	305	JEN11-1C-3	10.0	0.3	223	32	UH3-3	8.6	0.4
143	239	JEN11-1C-3	9.9	0.3	UH6-3 transect length: 531 μm				
144	100	JEN11-1C-3	9.9	0.3	213	531	UH6-3	8.2	0.4
142	15	JEN11-1C-3	10.2	0.3	217	394	UH6-3	7.3	0.4
146	28	JEN11-1C-3	10.1	0.3	216	263	UH6-3	7.8	0.4
145	71	JEN11-1C-3	9.6	0.3	215	156	UH6-3	7.9	0.4
JEN11-3C-1 transect length: 417 μm					214	38	UH6-3	7.7	0.4
230	417	JEN11-3C-1	11.6	0.3	UH12-5 transect length: 226 μm				
234	321	JEN11-3C-1	11.5	0.3	127	346	UH12-5	8.0	0.4
233	163	JEN11-3C-1	11.1	0.3	128	391	UH12-5	7.6	0.4
232	92	JEN11-3C-1	11.2	0.3	121	226	UH12-5	6.8	0.4
231	13	JEN11-3C-1	11.2	0.3	124	178	UH12-5	7.2	0.4
					123	130	UH12-5	7.5	0.4
					126	87	UH12-5	7.8	0.4
					125	48	UH12-5	7.8	0.4
					122	13	UH12-5	8.3	0.4

^a Distance between points based on a rim value of 0 μm measured perpendicular along transect from nearest euhedral edge

^b Last number in sample name indicates garnet number based on mount order. Off-transect points are indicated in italics. SIMS point locations are shown by white circles with black outlines in Figs. 4 and 5 and Appendix C on supplementary material. A detailed presentation of the SIMS data is in Appendix A on supplementary material

subset of eclogite garnet samples were selected for SIMS analysis (UH1, JEN11-1C, JEN11-1D, and JEN11-3C).

Oxygen isotopes by SIMS

A total of twelve eclogite garnets from the three localities were analyzed for oxygen isotope ratio using SIMS. Two garnets from Ring Mountain eclogite (UH1) decrease in $\delta^{18}\text{O}$ values (6.0 ± 0.3 ‰ to 3.8 ± 0.6 ‰) from core to rim (Fig. 4d, e). Two garnets from each of the three Mount Hamilton eclogite samples (MH8, MH9, and MH10) were analyzed using SIMS. All six garnets show a decrease in $\delta^{18}\text{O}$ values from core to rim. Garnets from MH8 and MH10 decrease from 8.6 ± 0.5 ‰ to 5.9 ± 0.6 ‰ (Fig. 4a, c). Garnets from MH9 decrease from 7.1 ± 0.2 ‰ to 5.7 ± 0.5 ‰ (Fig. 4b). Four Jenner Beach garnets were

analyzed using SIMS. Two are unzoned in oxygen isotope composition (JEN11-1C-3 = 11.4 ± 0.2 ‰ and JEN11-3C-1 = 9.9 ± 0.3 ‰) (Appendix C on supplementary material: a&b). The other two Jenner Beach garnets decrease in $\delta^{18}\text{O}$ value from core to rim. Garnet JEN11-3C-3 decreases from 11.0 ± 0.4 ‰ to 9.8 ± 0.2 ‰ (Appendix C on supplementary material: c), and JEN11-1D decreases from 11.3 ‰ to 10.2 ± 0.2 ‰ (Fig. 4f). A total of nine eclogite garnets show an abrupt decrease in $\delta^{18}\text{O}$ values between 80 and 150 μm from the rim. The three exceptions include garnet MH10-1 where the decrease occurs at ~ 310 μm from the rim and the two unzoned garnets from Jenner Beach. A summary of the SIMS analyses is provided in Table 3 and Fig. 3, and a detailed presentation is available in Appendix A on supplementary material.

Fig. 3 Chart summarizing the range of $\delta^{18}\text{O}$ values for bulk and SIMS data by location, mineralogy, and lithology. ^aUnzoned Jenner beach garnets are excluded. ^bRing Mountain amphibolite garnets UH3-1 and UH12-5. ^cRing Mountain amphibolite “U”-shaped garnets UH3-3 and UH6-3

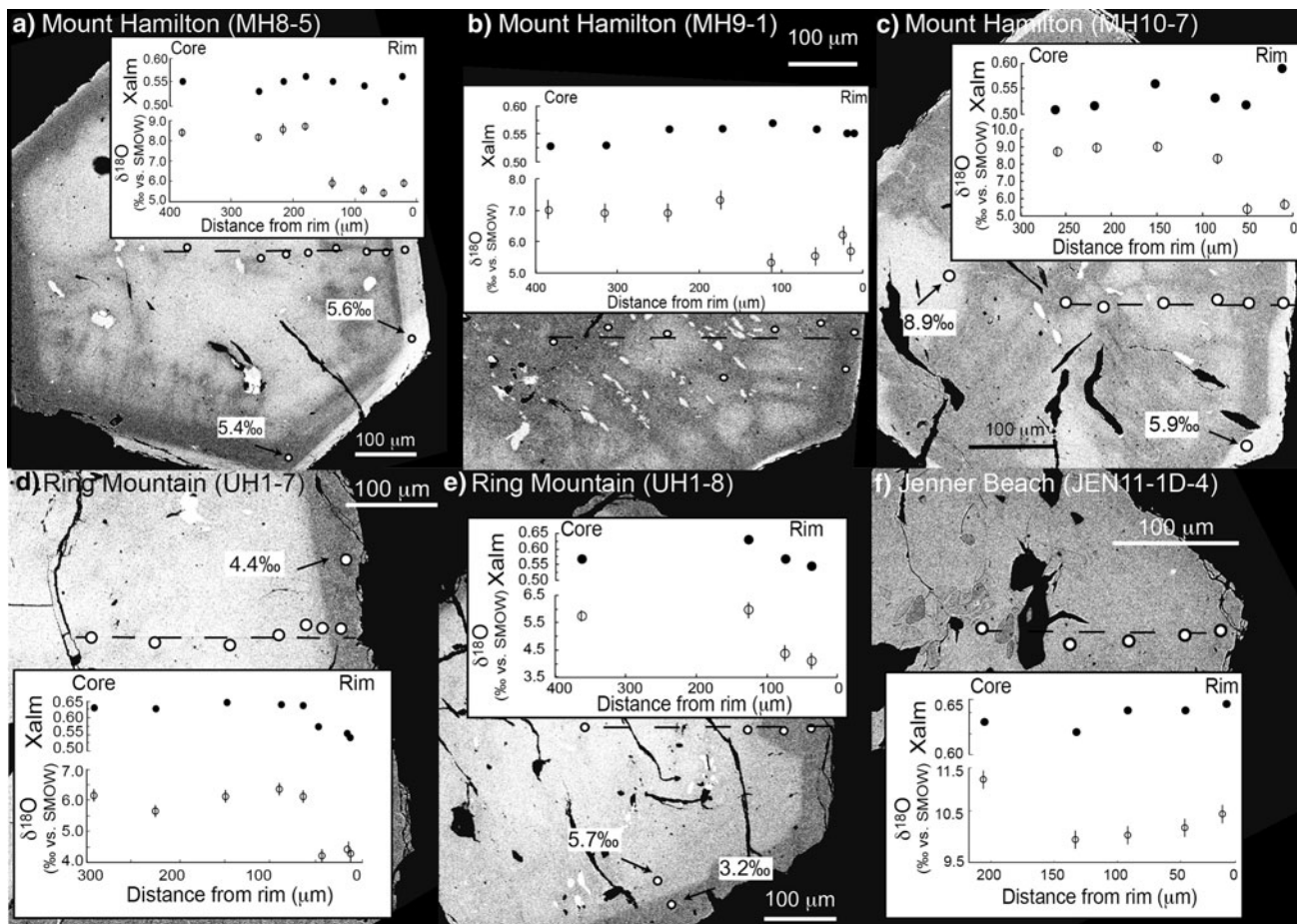
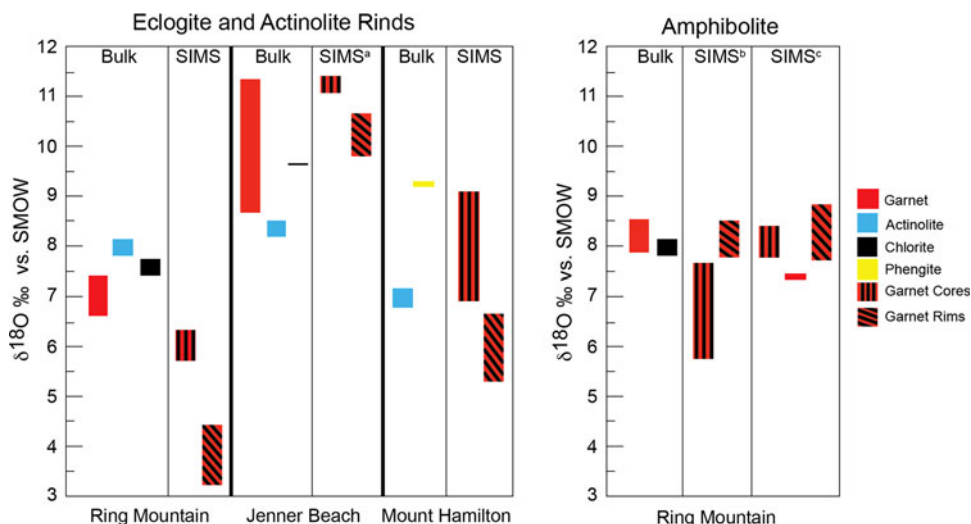


Fig. 4 BSE images of eclogite garnets from **a** Mount Hamilton (MH8-5), **b** Mount Hamilton (MH9-1), **c** Mount Hamilton (MH10-7), **d** Ring Mountain (UH1-7), **e** Ring Mountain (UH1-8), and **f** Jenner Beach (JEN11-1D-4), showing location of SIMS analyses and plots of

the mole fraction of almandine and the $\delta^{18}\text{O}$ value versus distance from the rim. *Black dashed lines* indicate transect trend, and *white circles with black outlines* indicate location of SIMS analyses

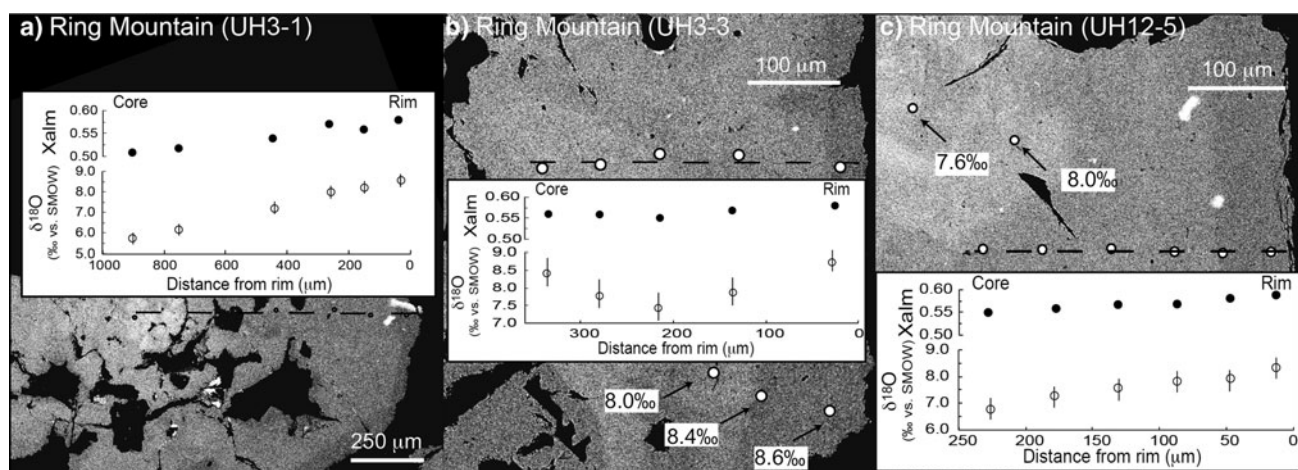


Fig. 5 BSE images of amphibolite garnets from **a** Ring Mountain (UH3-1), **b** Ring Mountain (UH3-3), and **c** Ring Mountain (UH12-5), showing location of SIMS analyses and plots of the mole fraction of

almandine and the $\delta^{18}\text{O}$ value versus distance from the rim. *Black dashed lines* indicate transect trend, and *white circles* indicate location of SIMS analyses

Amphibolite

Oxygen isotopes by laser fluorination

Bulk $\delta^{18}\text{O}$ values for garnets from five Ring Mountain amphibolite samples have a narrow range of 7.9–8.5 ‰ ($n = 8$) (Table 2; Fig. 3). A subset of samples were selected for ion microprobe analysis (UH3, UH6, and UH12). Their bulk $\delta^{18}\text{O}$ values are 8.3 ‰ ($n = 1$), 8.3 ± 0.1 ‰ ($n = 3$), and 8.5 ‰ ($n = 1$), respectively (Table 2).

Oxygen isotopes by SIMS

Ion microprobe analysis of four amphibolite garnets from Ring Mountain shows a general increase in $\delta^{18}\text{O}$ values from core to rim. For example, two garnets from UH3 were analyzed: UH3-1 steadily increases from 5.7 ‰ in the core to 8.5 ‰ at the rim, whereas UH3-3 has a $\delta^{18}\text{O}$ value of 8.4 ‰ in the core and drops to 7.4 ‰ at ~ 200 μm from the rim before increasing to 8.8 ‰ at the rim (Fig. 5a, b). The $\delta^{18}\text{O}$ value of UH12-5 increases from 6.8 ‰ in the core to 8.3 ‰ at the rim (Fig. 5c). Garnet UH6-3 has a similar horseshoe pattern as the second garnet from UH3-3 with a $\delta^{18}\text{O}$ value of 8.2 ‰ in the core dropping to 7.3 ‰ at 400 μm from the rim before increasing to 7.8 ‰ (Appendix C on supplementary material: g).

Actinolite rinds

Actinolite and chlorite bulk $\delta^{18}\text{O}$ values from the Ring Mountain eclogite block rind are +7.0 to +8.1 ‰ ($n = 3$) and +7.4 to +7.7 ‰ ($n = 2$), respectively and from the Jenner Beach eclogite block rind are +8.2 to +8.5 ‰ ($n = 2$) and +9.6 ‰, respectively. Actinolite and phengite

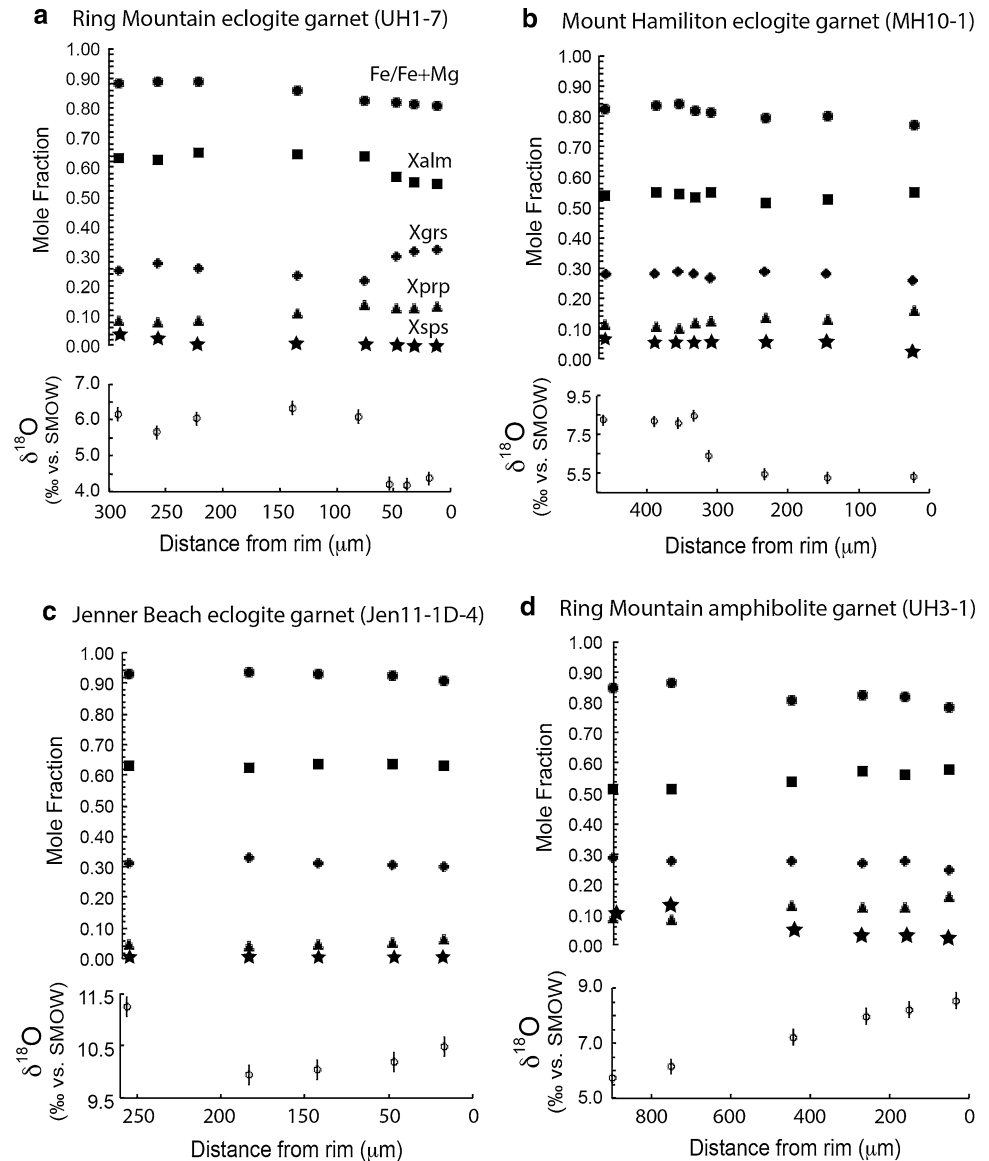
from the Mount Hamilton eclogite rind are +7.1 to +6.9 ‰ ($n = 3$) and +9.2 ‰ ($n = 1$), respectively (Table 2; Fig. 3).

Garnet major element geochemistry

Eclogite and amphibolite garnets were analyzed for Mg, Fe, Al, Si, Ca, Mn, and Cr concentrations adjacent to the SIMS spots. Three points were analyzed for each SIMS spot and average values calculated. The mole fractions of almandine (Xalm), pyrope (Xprp), grossular (Xgrs), and spessartine (Xsps) were calculated from oxide wt%. All garnets analyzed are almandine-rich with values of Xalm ranging from 0.51 to 0.66. The grossular component varies between 0.22 and 0.38 ± 0.05 . Concentrations of pyrope and spessartine are low with Xprp ranging from 0.04 to 0.18 and Xsps ranging from 0.00 to 0.13 (Appendix B on supplementary material). Major element zoning in the garnets from the three localities is highly varied. In general, most garnets show prograde growth with a steady decrease in the spessartine component and Fe/(Fe + Mg) ratio from core to rim and a marked increase in the pyrope component at the rim (Fig. 6, Appendix B on supplementary material). Xalm is highly varied, but generally has higher concentrations in the core compared to the rim. In some garnets, Xalm dramatically increases or decreases at the rim, and in others, it is relatively constant across the rim (Figs. 4, 5, 6, and Appendix B on supplementary material).

Correlations between in situ SIMS oxygen isotope zoning and major element zoning are not consistent. In some samples (e.g., UH1-7, Figs. 4d and 6a), the decrease in $\delta^{18}\text{O}$ values at the rims correlates with the decrease in Xalm and increase in Xgrs at the rim, while in other samples (e.g., MH8-5, Fig. 4a), the decrease in the $\delta^{18}\text{O}$

Fig. 6 The mole fractions of almandine (Xalm), pyrope (Xprp), grossular (Xgrs), and spessartine (Xsps), the Fe/Fe + Mg ratio and the $\delta^{18}\text{O}$ zoning profiles for three eclogite garnets (a–c) and one amphibolite garnet (d). Distance is measured from the rim on the right to the core on the left



value at the rim occurs closer to the core of the garnet compared with the increase in Xalm at the rim. Other samples (e.g., MH9-1, Fig. 4b) record a distinct decrease in the $\delta^{18}\text{O}$ value, yet the Xalm is relatively homogenous across the garnet. Other studies have noted inconsistent correlations between oxygen isotope and major element zoning in garnets with jumps in $\delta^{18}\text{O}$ value in some cases correlating with changing major element chemistry, likely linked to changing fluid composition, and in others a change in $\delta^{18}\text{O}$ value with homogeneous cation concentrations (e.g., Russell et al. 2013; D’Errico et al. 2012).

Discussion

Bulk garnet $\delta^{18}\text{O}$ values vary between locality, lithology, and metamorphic grade. Ring Mountain amphibolites

($+8.2 \pm 0.2$ ‰, $n = 7$, five samples) have a considerably higher $\delta^{18}\text{O}$ value than Ring Mountain eclogites ($+6.8 \pm 0.3$ ‰, $n = 4$, two samples). Among eclogites, Jenner Beach ($+9.8 \pm 0.7$ ‰, $n = 11$, five samples) is on average 3.0 ‰ greater in $\delta^{18}\text{O}$ (garnet) than Ring Mountain. All samples are higher in $\delta^{18}\text{O}$ than unaltered MORB ($\delta^{18}\text{O}(\text{WR}) = +5.5$ ‰, Eiler 2001). We suggest that these higher $\delta^{18}\text{O}$ values reflect variable low-temperature sea-floor alteration in the basaltic protolith prior to subduction (Gregory and Taylor 1981).

Eclogites

Ion microprobe analysis of nine eclogite garnets reveals a $\sim 1\text{--}3$ ‰ decrease in $\delta^{18}\text{O}$ values from the core to the rim of the garnet with a distinct drop in the $\delta^{18}\text{O}$ value $\sim 120 \pm 50$ μm from the rim regardless of garnet size

(radii varying from ~ 250 to $750 \mu\text{m}$) (Fig. 4). Bulk $\delta^{18}\text{O}$ values of Jenner Beach eclogite garnets are consistent with the $\delta^{18}\text{O}$ values of the garnet cores. One Ring Mountain sample has a $\sim 0.5 \text{‰}$ higher bulk value than the core of the two garnets analyzed via ion microprobe. This may be due to isotopic variability among the garnets; however, it is close to the analytical uncertainty of the ion microprobe (0.3‰); therefore, it is difficult to draw a meaningful conclusion. Although we suggest that the higher $\delta^{18}\text{O}$ value in the cores of the garnet reflects the original isotopic composition of the hydrothermally altered basaltic protolith, as has been commonly proposed in other orogenic and subduction zone eclogites (Russell et al. 2013; Putlitz et al. 2000; Halama et al. 2011; Barnicoat and Cartwright 1995), we cannot completely rule out a possible sedimentary-derived fluid component during early prograde garnet growth.

The lower $\delta^{18}\text{O}$ value of eclogite garnet rims may be due to either: (1) the fractionation of oxygen isotopes with changing temperatures during garnet growth or (2) interaction with a lower $\delta^{18}\text{O}$ fluid. A gradual change in $\delta^{18}\text{O}$ values is expected from changing temperatures during garnet growth; however, the observed variation is larger than can be attributed to changing temperature during closed-system mineral growth. Assuming garnet growth from 450 to 600 °C and a biminerally assemblage with equal modal abundance of garnet and omphacite, the variation in $\delta^{18}\text{O}$ value will be significantly $< 1.0 \text{‰}$ given the small oxygen isotope fractionation between garnet and pyroxene at high temperatures. The observed abrupt and larger than 1‰ decrease in the $\delta^{18}\text{O}$ values of the garnet rims compared to the cores suggests a rapid change in fluid composition at the end of prograde garnet growth. The involvement of an external fluid is consistent with the observations by Russell et al. (2013) who note in a survey study of oxygen isotope zoning eclogitic garnets from five different locations that nine out of the 12 garnets analyzed require external fluid infiltration to account for the change in oxygen isotope composition across the garnet.

Large-ion lithophile element enrichments and Nd and Sr isotope compositions suggest that a major component of the fluids responsible for blueschist facies overprinting of high-grade blocks was sediment derived (Nelson 1991, 1995; Sorensen et al. 1997; Horodyskyj et al. 2009); however, temperature estimates for overprinting of Franciscan blueschist facies minerals are far too low for garnet growth. Furthermore, fluids derived from dehydrating sediments during subduction typically have high $\delta^{18}\text{O}$ values ($\sim 10\text{--}30 \text{‰}$; Sharp (2007) and references therein). At eclogite facies temperatures, an alternate source is required to account for the lower $\delta^{18}\text{O}$ value of the garnet rims. There is minimal oxygen isotope fractionation during metamorphic dehydration reactions (e.g., Valley 1986);

therefore, the potential fluid source will have a low $\delta^{18}\text{O}$ value.

We suggest that the lower $\delta^{18}\text{O}$ value of garnet rims reflects the oxygen isotope composition of the surrounding serpentinized mantle wedge. Typical oceanic serpentinites have $\delta^{18}\text{O}$ values between ~ 0 and 6‰ (e.g., Wenner and Taylor 1974). At the initiation of subduction while eclogite facies temperatures persist, fluid-mediated exchange between the mantle wedge and the underplated blocks could explain the lower $\delta^{18}\text{O}$ value of the garnet rims. Since the volume of ultramafic rock in the mantle wedge is potentially much greater than that of infiltrating slab-derived fluids, the oxygen isotope composition of the fluids is partly buffered by the surrounding ultramafic rock. The lower $\delta^{18}\text{O}$ value of the surrounding ultramafic rock is recorded in the final stages of garnet growth.

Actinolite rinds

The association between serpentinite and Franciscan high-grade blocks is commonly proposed based on the preserved actinolite rinds encasing the blocks. Although direct serpentinite block contacts are not documented in the Franciscan, metasomatic rinds are preserved on mafic blocks in contact with ultramafic matrix in Syros and Catalina (e.g., Breeding et al. 2004; Bebout and Barton 2002). This association with serpentinite is a main line of evidence invoked to support serpentinite diapirism as a mode of exhumation for the blocks (Moore 1984; Cloos 1986; Coleman and Lanphere 1971; Giaramita and Sorensen 1994; Horodyskyj et al. 2009); however, the timing and mechanism of this association are not well constrained. The high Mg, Ni, and Cr contents of the rinds suggest that the rind itself is replaced ultramafic material that forms as a reaction zone between the high-grade block and surrounding ultramafic rock (Cloos 1986). $^{187}\text{Os}/^{186}\text{Os}$ ratios and HSE (Os, Ir, Ru, Pt, Pd, Re) abundances are also similar between the rinds and typical mantle peridotite suggesting either a fluid-mediated transfer or more likely mechanical mixing with the peridotite host (Penniston-Dorland et al. 2012). Block rinds are primarily actinolite, but also contain varying amounts of chlorite and white mica (Nelson 1991, 1995; Sorensen et al. 1997; Penniston-Dorland et al. 2010). Coexisting mineral pairs of actinolite and white mica from the Mount Hamilton rind and actinolite-chlorite from the Ring Mountain rind, assuming equilibration, yield oxygen isotope temperatures of $185\text{--}240 \text{ °C}$ (Zheng 1993; Wenner and Taylor 1971). Actinolite-chlorite oxygen isotope thermometry from the Jenner Beach rinds yields lower temperatures ($135\text{--}150 \text{ °C}$). These temperature estimates are slightly lower than Moore's (1984) rind temperature estimate of $250\text{--}300 \text{ °C}$ using Fe–Mg thermometry between chlorite

and actinolite on the Mount Hamilton eclogite block. These temperatures are much too low for garnet growth and blueschist facies overprinting, suggesting that rind formation was a temporally later stage of block retrogression. It is possible that rind formation started earlier in the blocks history and involved multiple stages. The temperatures recorded in the chlorite and actinolite may only represent the final stages of rind formation. However, if we use the temperatures calculated here and the average $\delta^{18}\text{O}$ value of the actinolite in the respective rinds, the actinolite is in isotopic equilibrium with serpentine with $\delta^{18}\text{O}$ values of 6.6–7.6 ‰ (Wenner and Taylor 1971; Zheng 1993). These values overlap well with reported $\delta^{18}\text{O}$ values of serpentine at Ring Mountain and Tiburon Peninsula (+6.0 to +8.1 ‰) (Barnes et al. 2013; Wenner and Taylor 1974) supporting interaction with serpentinite either through mechanical mixing or through fluid-mediated transfer during rind formation.

Ring Mountain amphibolites

The Ring Mountain amphibolite garnets show a more complex oxygen isotope zoning pattern than the eclogites. All four garnets come from a single amphibolite block yet show inconsistent patterns. Amphibolite garnets UH3-3 and UH6-3 show a “U”-shaped pattern with the highest $\delta^{18}\text{O}$ values in the core and at the rim, whereas UH3-1 and UH12-5 show a gradual increase in $\delta^{18}\text{O}$ value from core to rim (Fig. 5 and Appendix C on supplementary material). One explanation for these complexities is that the points analyzed in garnets UH3-3 and UH6-3 did not represent true core to rim transects. If the traverse represents an incomplete rim-to-core-to-rim traverse, then all the amphibolite garnets would show a gradual increase in the $\delta^{18}\text{O}$ value from core to rim. Lu–Hf geochronology from a garnet amphibolite block from Panoche Pass yields a slightly older age (~169–162 Ma) than the eclogites (~159–153 Ma), suggesting amphibolite peak metamorphism near the time of subduction initiation (Anczkiewicz et al. 2004). The disparate oxygen isotope trends and ages suggest different tectonic histories for the eclogite and amphibolite blocks. The higher $\delta^{18}\text{O}$ values at the rims of the amphibolite garnets could be explained by interaction with a sediment-derived fluid during garnet growth. If the amphibolite block reached peak metamorphic conditions prior to the eclogites or earlier in the life of the subduction zone, it may have interacted with an early influx of sediment-derived fluids. However, we do note that an eclogite overprinted amphibolite from Ring Mountain has a similar age to an eclogite from Ring Mountain (Anczkiewicz et al. 2004), stressing the need for additional, and if possible correlated, oxygen isotope and geochronologic studies of Franciscan amphibolites in order to understand how the

amphibolite blocks fit in the tectonic history of the Franciscan subduction zone.

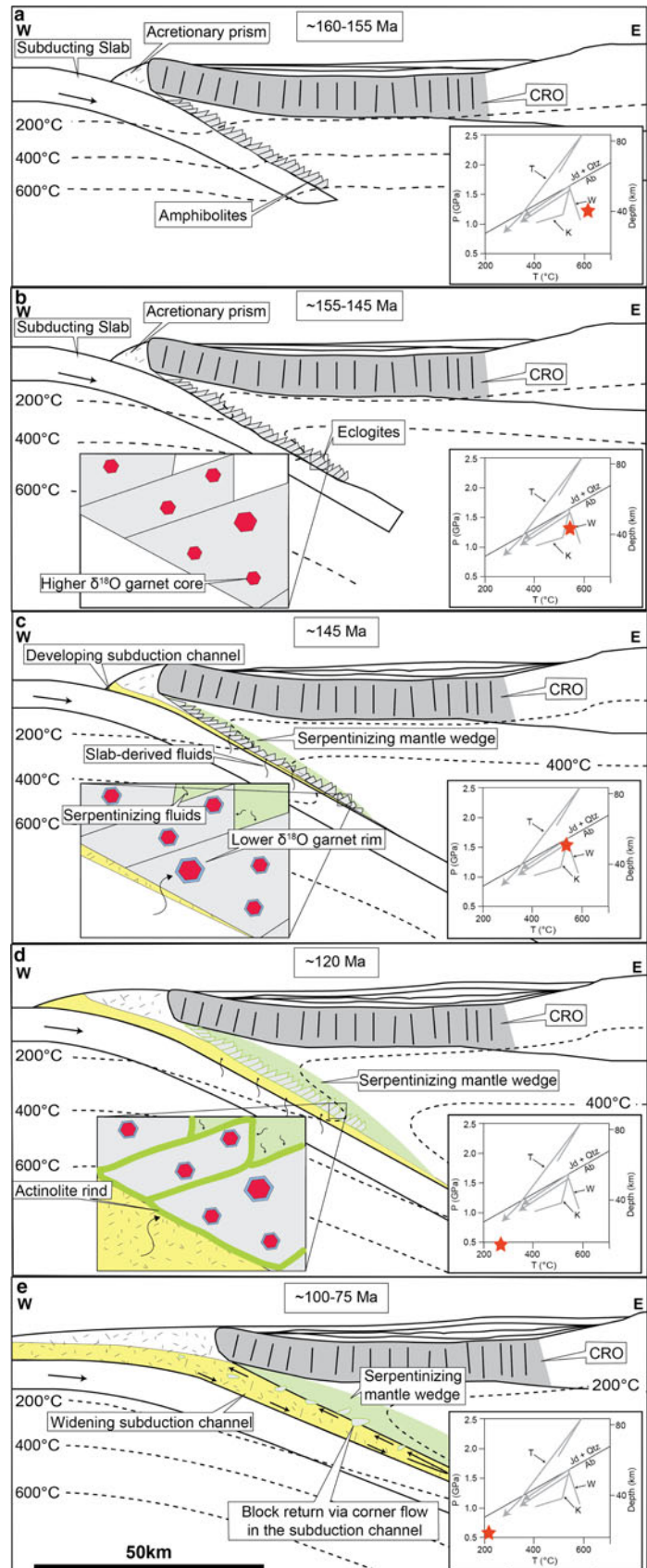
Tectonic model

To explain the observed trends in bulk and in situ oxygen isotope data, we suggest the following tectonic model (Fig. 7). At initiation of subduction, pieces of the down-going oceanic crust were fluxed with sediment-derived fluids after reaching amphibolite facies conditions as evidenced by the ^{18}O -enriched garnet rims compared to the cores (Fig. 7a). As subduction continued, additional blocks of oceanic crust were underplated in the mantle wedge soon after reaching peak eclogite conditions (Fig. 7b). The $\delta^{18}\text{O}$ values of eclogite garnet cores reflect the initial $\delta^{18}\text{O}$ values of the subducting altered oceanic crust (Gregory and Taylor 1981). Oxygen isotope exchange between the blocks and the partially serpentinized mantle wedge via slab-derived fluids results in lower $\delta^{18}\text{O}$ garnet rims (Fig. 7c). With a decreasing geothermal gradient from continued subduction, the blocks develop a retrograde blueschist facies overprint under relatively static conditions as is evidenced by pseudomorphic replacement of garnets by chlorite. Actinolite rind forms as infiltration of slab-derived fluids serpentinizes the mantle wedge inducing reaction between the blocks and surrounding ultramafic rocks (Fig. 7d). The blocks are then separated from the mantle wedge along the actinolite rind, a zone of weakness, and incorporated into the subduction channel where they flow back to the surface via corner flow (Fig. 7e) (Cloos 1986). This model presents a scenario in which eclogite blocks interacted with serpentinite, but does not dictate uplift in a serpentine diapir, conforming with the lack of observed block–serpentine contact in the Franciscan Complex.

Summary

In situ ion microprobe oxygen isotope analysis of Franciscan garnet cores and rims provides new insights into the timing and mechanism by which the blocks become associated with ultramafic rocks. The abrupt and larger than 1 ‰ decrease in $\delta^{18}\text{O}$ values from core to rim of the eclogite garnets suggests a rapid change in the oxygen isotope composition of fluids in equilibrium with the garnets during the final stages of growth. We attribute this decrease in the $^{18}\text{O}/^{16}\text{O}$ ratio at the garnet rim to the lower $\delta^{18}\text{O}$ value of the partly serpentinized mantle wedge. Actinolite rind formation temperatures together with the lower $\delta^{18}\text{O}$ garnet rims suggest that the blocks were in contact with ultramafic rock beginning at the end of garnet growth through low-temperature retrogression.

Fig. 7 Schematic diagram depicting: **a** Amphibolite metamorphism during the initial stages of subduction ~ 160 Ma, **b** underplating of ocean basalts with metamorphism to eclogite ~ 155 Ma, **c** final stage of eclogite garnet growth with blocks in the mantle wedge, **d** actinolite rind formation in serpentinizing mantle wedge (*green*), **e** erosion of high-grade blocks into widening subduction channel (*yellow*). Blocks and garnets are not to scale. Modified from Cloos (unpub) and Ukar (2012). *Gray arrows* indicate P–T paths from: T = Tsujimori et al. (2006), W = Wakabayashi (1990), K = Krogh et al. (1994). *Stars* indicate the general location of the model stage in P–T space



Acknowledgments We thank C.-T. Lee and M. Cloos for providing samples; R. Eldam and T. Prather for help with sample collection; and M. Cisneros for help with the EMP. The authors thank an unnamed reviewer and Zeb Page for their very thoughtful comments that contributed greatly to the improvement of this manuscript and Tim Grove for editorial handling. This research was supported by the Jackson School of Geosciences. N. Kita, T. Ushikubo, K. Kitajima, and J. Kern assisted in SIMS analysis. WiscSIMS is partly supported by NSF-EAR-1053466.

References

- Anczkiewicz R, Platt J, Thirlwall M, Wakabayashi J (2004) Franciscan subduction off to a slow start: evidence from high-precision Lu–Hf garnet ages on high grade-blocks. *Earth Planet Sci Lett* 225:147–161
- Bailey EH, Irwin WP (1959) K-feldspar content of Jurassic and Cretaceous graywackes of northern coast ranges and Sacramento Valley, California. *Am Assoc Pet Geol Bull* 43:2797–2809
- Bailey EH, Irwin WP, Jones DL (1964) Franciscan and related rocks and their significance in the geology of western California. *Calif Div Mines Bull* 183:1–177
- Barnes JD, Eldam R, Lee C-T, Errico JC, Loewy SL, Cisneros M (2013) Petrogenesis of serpentinites from the Franciscan Complex, western California, USA. *Lithos*. <http://dx.doi.org/10.1016/j.lithos.2012.12.018>
- Barnicoat AC, Cartwright I (1995) Focused fluid flow during subduction: oxygen isotope data from high-pressure ophiolites of the western Alps. *Earth Planet Sci Lett* 132:53–61
- Bebout GE, Barton MD (1989) Fluid flow and metasomatism in a subduction zone hydrothermal system: Catalina Schist terrane, California. *Chem Geol* 17:976–980
- Bebout GE, Barton MD (1993) Metasomatism during subduction: products and possible paths in the Catalina Schist, California. *Chem Geol* 108:61–92
- Bebout GE, Barton MD (2002) Tectonic and metasomatic mixing in a high-T, subduction-zone mélangé—insights into the geochemical evolution of the slab–mantle interface. *Chem Geol* 187:79–106
- Blake MC, Jayko AS, McLaughlin RJ, Underwood MB (1988) Metamorphic and tectonic evolution of the Franciscan Complex, Northern California. *Metamorph Crustal Evol West US* 38:1036–1060
- Breeding CM, Ague JJ, Brocker M (2004) Fluid–metasedimentary rock interactions in subduction-zone mélangé: implications for the chemical composition of arc magmas. *Geology* 32:1041–1044
- Catlos E, Sorensen SS (2003) Phengite-based chronology of K- and Ba-Rich fluid flow in two paleosubduction zones. *Science* 299:92–95
- Cloos M (1982) Flow melanges: numerical modeling and geologic constraints on their origin in the Franciscan subduction complex, California. *Geol Soc Am Bull* 93:330–345
- Cloos M (1985) Thermal evolution of convergent plate margins: thermal modeling and reevaluation of isotopic Ar-ages for blueschists in the Franciscan Complex of California. *Tectonics* 4:421–433
- Cloos M (1986) Blueschists in the Franciscan Complex of California: petrotectonic constraints on uplift mechanisms. *Geol Soc Am Mem* 164:77–93
- Coleman R, Lanphere M (1971) Distribution and age of high-grade blueschists, associated eclogites, and amphibolites from Oregon and California. *Geol Soc Am Bull* 82:2397–2412
- Compton R (1962) *Geology in the field*. Wiley, New Jersey, pp 1–398
- D’Errico M, Lackey JS, Surpless B, Loewy S, Wooden J, Barnes JD, Strickland A, Valley JW (2012) A detailed record of shallow hydrothermal fluid flow in the Sierra Nevada magmatic arc from low- $\delta^{18}\text{O}$ skarn garnets. *Geology* 40:763–766
- Donovan JJ, Kremser D, Fournelle JH (2007) *Probe for windows user’s guide and reference*, Enterprise edn. Probe Software, Inc., Eugene, OR, pp 1–355
- Eiler J (2001) Oxygen isotope variations of basaltic lavas and upper mantle rocks. *Rev Mineral Geochem* 43:319–364
- Ernst W (1970) Tectonic contact between the Franciscan melange and the Great Valley sequence—crustal expression of a late Mesozoic Benioff zone. *J Geophys Res* 75(5):886–901
- Giaramita M, Sorensen S (1994) Primary fluids in low-temperature eclogites: evidence from two subduction complexes (Dominican Republic, and California, USA). *Contrib Mineral Petrol* 117:279–292
- Gregory RT, Taylor HP Jr (1981) An oxygen isotope profile in a section of Cretaceous oceanic crust, Samail ophiolite, Oman: evidence for $\delta^{18}\text{O}$ buffering of the oceans by deep (>5 km) seawater-hydrothermal circulation at mid-ocean ridges. *J Geophys Res* 86 B4:2737–2755
- Halama R, John T, Herms P, Hauff F, Schenk V (2011) A stable (Li, O) and radiogenic (Sr, Nd) isotope perspective on metasomatic processes in a subducting slab. *Chem Geol* 281(3–4):151–166
- Hamilton W (1969) Mesozoic California and the underflow of pacific mantle. *Geol Soc Am Bull* 80:2409–2429
- Harms TA, Jayko AS, Blake MC (1992) Kinematic evidence for extensional unroofing of the Franciscan complex along the Coast Range fault, northern Diablo Range, California. *Tectonics* 11:228–241
- Herrington KL (1985) Metamorphism, deformation and alteration of an eclogite block from the Franciscan subduction complex, central California. M.A. Thesis (Cloos, M.)
- Horodyskyj U, Lee C, Luffi P (2009) Geochemical evidence for exhumation of eclogite via serpentinite channels in ocean-continent subduction zones. *Geosphere* 5:426–438
- Jayko AS, Blake MC, Harms T (1987) Attenuation of the coast range ophiolite by extensional faulting, and nature of the coast range “Thrust”, California. *Tectonics* 6:475–488
- Kita NT, Ushikubo T, Fu B, Valley JW (2009) High precision SIMS oxygen isotope analysis and the effect of sample topography. *Chem Geol* 264:43–57
- Krogh Ravna EJ, Terry MP (2004) Geothermobarometry of UHP and HP eclogites and schists—an evaluation of equilibria among garnet–clinopyroxene–kyanite–phengite–coesite/quartz. *J Metamorph Geol* 22(6):579–592
- Krogh E, Oh C, Liou J (1994) Polyphase and anticlockwise P–T evolution for Franciscan eclogites and blueschists from Jenner, California, USA. *J Metamorph Geol* 12:121–134
- Moore D (1984) Metamorphic history of a high-grade blueschist exotic block from the Franciscan Complex, California. *J Petrol* 25:126–150
- Moore DE, Blake MC (1989) New evidence for polyphase metamorphism of glaucophane schist and eclogite exotic blocks in the Franciscan Complex, California and Oregon. *J Metamorph Geol* 7:211–228
- Nelson B (1991) Sediment-derived fluids in subduction zones: isotopic evidence from veins in blueschist and eclogite of the Franciscan Complex, California. *Geology* 19:1033–1036
- Nelson B (1995) Fluid flow in subduction zones: evidence from Nd- and Sr-isotope variations in metabasalts of the Franciscan complex, California. *Contrib Mineral Petrol* 119:247–262
- Page NJ (1968) Serpentinization in a sheared serpentinite lens Tiburon Peninsula, California. *US Geol Surv Prof Pap* 600B:21–28

- Page FZ, Armstrong L, Essene E (2007) Prograde and retrograde history of the Junction School eclogite, California, and an evaluation of garnet–phengite–clinopyroxene thermobarometry. *Contrib Mineral Petrol* 153:533–555
- Page FZ, Kita NT, Valley JW (2010a) Ion microprobe analysis of oxygen isotopes in garnets of complex chemistry. *Chem Geol* 270:9–19
- Page FZ, Essene EJ, Kita NT, Valley JW (2010b) Cryptic metasomatism during exhumation of Franciscan eclogite and hornblende revealed by in situ $\delta^{18}\text{O}$ analysis of garnets. 20th Annual Goldschmidt Conference, *Geochim Cosmochim Acta* 74: Suppl. A785
- Penniston-Dorland SC, Sorensen SS, Ash RD, Khadke SV (2010) Lithium isotopes as a tracer of fluids in a subduction zone mélange: Franciscan Complex, CA. *Earth Planet Sci Lett* 292:181–190
- Penniston-Dorland SC, Walker RJ, Pitcher L, Sorensen SS (2012) Mantle–crust interactions in a paleosubduction zone: evidence from highly siderophile element systematics of eclogite and related rocks: earth planet. *Sci Lett* 319–320:295–306
- Pincus MR, Page FZ, Spicuzza MJ, Valley JW (2010) Widespread oxygen isotope disequilibrium in Franciscan high-grade blocks. *Geol Soc Am Abstr Progr* 42:629
- Platt J (1986) Dynamics of orogenic wedges and the uplift of high-pressure metamorphic rocks. *Geol Soc Am Bull* 97:1037–1053
- Putlitz B, Matthews A, Valley JW (2000) Oxygen and hydrogen isotope study of high-pressure metagabbros and metabasalts (Cyclades, Greece): implications for the subduction of oceanic crust. *Contrib Mineral Petrol* 138(2):114–126
- Ring U, Brandon M (1994) Kinematic data for the coast range fault and implications for exhumation of the Franciscan subduction complex. *Geology* 22:735–738
- Russell AK, Kitajima K, Strickland A, Medaris LG, Schulze DJ, Valley JW (2013) Eclogite-facies fluid infiltration: constraints from $\delta^{18}\text{O}$ zoning in garnet. *Contrib Mineral Petrol* 165:103–116
- Schemmann K, Unruh J, Moores EM (2008) Kinematics of Franciscan Complex exhumation: new insights from the geology of Mount Diablo, California. *Geol Soc Am Bull* 120:543–555
- Sharp ZD (1990) A laser-based microanalytical method for the in situ determination of oxygen isotope ratios of silicates and oxides. *Geochim Cosmochim Acta* 54:1353–1357
- Sharp ZD (2007) Principles of stable isotope geochemistry. Pearson Prentice Hall, Upper Saddle River, pp 1–344
- Simons KK, Harlow GE, Brueckner HK, Goldstein SL, Sorensen SS, Hemming NG, Langmuir CH (2010) Lithium isotopes in Guatemalan and Franciscan HP-LT rocks: insights into the role of sediment-derived fluids during subduction. *Geochim Cosmochim Acta* 74:3621–3641
- Sorensen S, Grossman J, Perfit MR (1997) Phengite-hosted LILE enrichment in eclogite and related rocks: implications for fluid-mediated mass transfer in subduction zones and arc magma genesis. *J Petrol* 38:3–34
- Spandler C, Hermann J, Arculus R, Mavrogenes J (2004) Geochemical heterogeneity and element mobility in deeply subducted oceanic crust; insights from high-pressure mafic rocks from New Caledonia. *Chem Geol* 206:21–42
- Taylor HP, Coleman RG (1968) $\text{O}^{18}/\text{O}^{16}$ ratios of coexisting minerals in glaucophane-bearing metamorphic rocks. *Geol Soc Am Bull* 79:1727–1755
- Tsujimori T, Matsumoto K, Wakabayashi J, Liou JG (2006) Franciscan eclogite revisited: reevaluation of the P–T evolution of tectonic blocks from Tiburon Peninsula, California, USA. *Miner Petrol* 88:243–267
- Ukar E (2012) Tectonic significance of low-temperature blueschist blocks in the Franciscan mélange at San Simeon, California. *Tectonophysics* 568–569:154–169
- Valley JW (1986) Stable isotope geochemistry of metamorphic rocks. *Rev Miner* 16:445–489
- Valley JW, Kita NT (2009) In situ oxygen isotope geochemistry by ion microprobe. *Miner Assoc Can Short Course* 41:19–63
- Valley JW, Kitchen N, Kohn M, Niendorf C (1995) UWG-2, a garnet standard for oxygen isotope ratios: strategies for high precision and accuracy with laser heating. *Geochim Cosmochim Acta* 59:5223–5231
- Wakabayashi J (1990) Counterclockwise PTt paths from amphibolites, Franciscan Complex, California: relics from the early stages of subduction zone metamorphism. *J Geol* 98:657–680
- Wenner DB, Taylor HP (1971) Temperatures of serpentinization of ultramafic rocks based on $\text{O}^{18}/\text{O}^{16}$ Fractionation between coexisting serpentine and magnetite. *Contrib Mineral Petrol* 32:165–185
- Wenner DB, Taylor HP (1974) D/H and $\text{O}^{18}/\text{O}^{16}$ studies of serpentinization of ultramafic rocks. *Geochim Cosmochim Acta* 38:1255–1286
- Zheng Y-F (1993) Calculation of oxygen isotope fractionation in anhydrous silicate minerals. *Geochim Cosmochim Acta* 57:1079–1091